Automated quantification of morphodynamics for high-throughput live cell time-lapse dataset

Gonzalez, German ; Fusco, Ludovico ; Benmansour, Fethallah ; Fua, Pascal ; Pertz, Olivier ; Smith, Kevin

AUTOMATED QUANTIFICATION OF MORPHODYNAMICS FOR HIGH-THROUGHPUT LIVE CELL TIME-LAPSE DATASETS

Germán González[1], *Ludovico Fusco*[2], *Fethallah Benmansour*[3], *Pascal Fua*[3], *Olivier Pertz*[2], *Kevin Smith*[4]

[1] Research Laboratory of Electronics, MIT [2] Institute of Biochemistry, University of Basel
[3] Computer Vision Lab, EPFL [4] Light Microscopy and Screening Center, ETHZ

ABSTRACT

We present a fully automatic method to track and quantify the morphodynamics of differentiating neurons in fluorescence time-lapse datasets. Previous high-throughput studies have been limited to static analysis or simple behavior. Our approach opens the door to rich dynamic analysis of complex cellular behavior in high-throughput time-lapse data. It is capable of robustly detecting, tracking, and segmenting all the components of the neuron including the nucleus, soma, neurites, and filopodia. It was designed to be efficient enough to handle the massive amount of data from a high-throughput screen. Each image is processed in approximately two seconds on a notebook computer. To validate the approach, we applied our method to over 500 neuronal differentiation videos from a small-scale RNAi screen. Our fully automated analysis of over 7,000 neurons quantifies and confirms with strong statistical significance static and dynamic behaviors that had been previously observed by biologists, but never measured.

Index Terms— Molecular and cellular screening; Image sequence processing; Fluorescence microscopy

1. INTRODUCTION AND RELATED WORK

The process of forming functional connections between neurons is complex and dynamic. Time-lapse microscopy has revealed that differentiating neurons undergo a large range of dynamic processes including cell body motility, filopodial dynamics, and repeated cycles of neurite growth and retraction. Of critical importance is the process by which axons and dendrites are formed in which a neurite ceases retracting, extends a long distance, and forms a connection. Such dynamic events are governed by a complex protein network that coordinates dynamic functions within the cytoskeleton, membrane, etc.

Powerful tools such as RNA interference (RNAi) technology, fluorescent protein labeling, image processing, and automated high-throughput microscopy have opened the door for large scale perturbation studies to help investigate such processes. RNAi screens have already led to novel insights into a number of cellular processes such as cell migration [1] and endocytosis [2]. However, limitations in image processing have restricted most investigations to static image analysis.

Knowledge of dynamics is essential if we are to understand complex processes such as neuron morphogenesis. However, designing algorithms to quantify dynamic behaviors is challenging, and automatic methods have appeared only very recently. State-of-the-art high-throughput techniques have successfully quantified morphodynamics of HeLA cancer cells in an effort to understand mitosis [3, 4] However, the morphology and dynamics of cells in previous studies are simple compared to neurons, whose highly deformable neurites that branch, expand, retract, and collapse.

In this paper, we propose a fully automatic method to detect, track, and segment *every component of the neuron* (nucleus, soma, neurites, and filopodia), as well as quantify their dynamic behaviors in ways that were previously not possible. Our approach begins with a tracking step that detects nuclei at each time step and associates nuclei belonging to the same neuron throughout the time-lapse sequence. Using tracked nuclei as seed points, a region-growing algorithm segments the neuron's soma. The somata are used to initialize a joint segmentation of the entire structure of all neurons in an image using a probabilistic method based on shortest path computations. A graph describing the morphology of the neurites is extracted from this segmentation. Each neurite tree is tracked by association, and filopodia are detected by analyzing the topology of the tracked neurites. Finally, a set of 156 morphodynamic features is extracted, quantifying the behavior of the each neuron in the video.

As demonstrated in Fig. 1, our approach extracts the neurons' dynamic morphology accurately and reliably. To validate our approach, we ran our algorithm on a small-scale siRNA screen of 5 genes (3 siRNAs/gene). Our analysis confirmed steady-state phenotypes obtained previously using MetaMorph™ [5]. We also quantified dynamic behaviors that were previously observed, but never measured [5], and uncovered new behaviors which are only apparent through dynamic analysis.

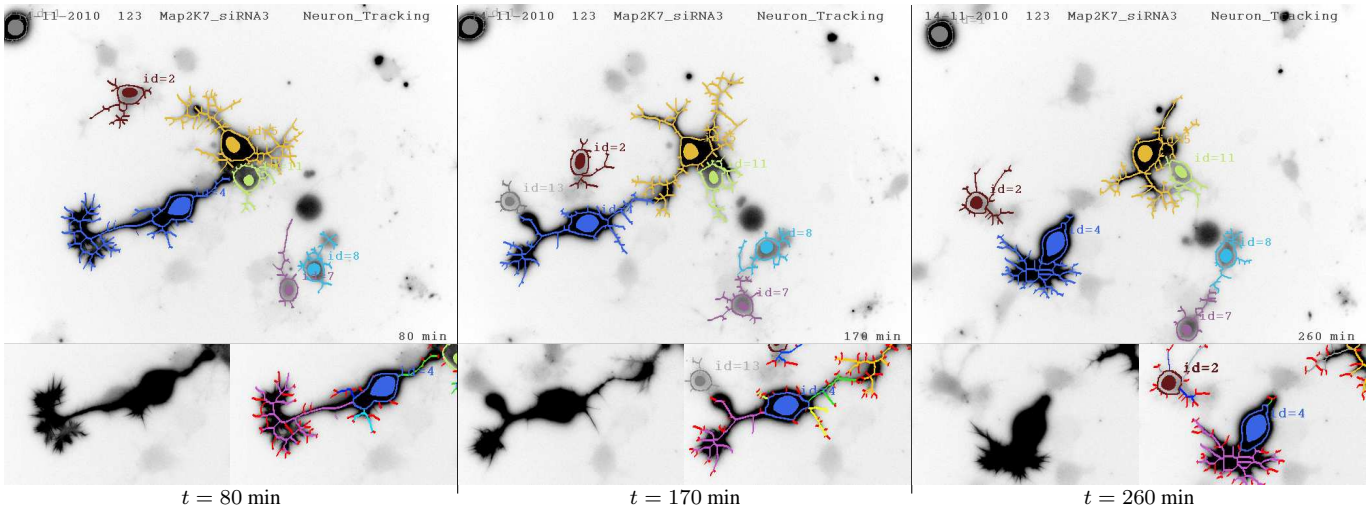

$t = 80$ min $t = 170$ min $t = 260$ min

Fig. 1: Our approach tracks and extracts the morphology of the entire neuron. The top row contains results from an experiment with inhibited MAP2K7 function. Tracked neurons are marked by a unique color and id. Nuclei are denoted by filled ellipsoids, somata as contours, and neurites as trees. The bottom shows details from above: the original image on the left and neurites marked with various colors on the right. Filopodia are marked in red. Our approach performs well even in challenging situations where neurons appear in close proximity. Note: contrast has been enhanced for visibility. Cells deemed uninteresting by the biologist (e.g. faint staining or a short lifetime) can optionally be ignored by the system to improve measurement quality.

2. HIGH-THROUGHPUT TRACKING AND SEGMENTATION

The input to our approach is a series of T images $\mathcal{I} = \{I_1, \ldots, I_t, \ldots, I_T\}$ from which we extract K nucleus detections d_t^k. The tracking step described in Sec. 2.2 associates valid detections across time steps while rejecting spurious detections. Since each neuron contains only one nucleus, there is a one-to-one mapping between each valid nucleus detection c_t^i and a neuron X_t^i. Thus, the tracking task is to provide a set of neuron detections $\mathcal{X}^i = \{X_a^i, \ldots, X_t^i, \ldots, X_b^i\}$ defining an individual neuron i from time $t = a$ to $t = b$. As depicted in Fig. 2, each neuron detection X_t^i is composed of a nucleus c_t^i, a soma s_t^i, a set of J neurites $\{n_t^{i,1}, \ldots, n_t^{i,j}, \ldots, n_t^{i,J}\}$, and a set of L filopodia associated with each neurite $F_t^{i,j} = \{f_t^{i,j,1}, \ldots, f_t^{i,j,l}, \ldots, f_t^{i,j,L}\}$ so that $N_t^i = \{(n_t^{i,1}, F_t^{i,1}), \ldots, (n_t^{i,j}, F_t^{i,j})\}$. Thus, a complete neuron i at time step t is described by $X_t^i = \{c_t^i, s_t^i, N_t^i\}$.

2.1. Nuclei and Somata Detection and Segmentation

The first step in our approach is to extract a set of nucleus detections $\{d^1, \ldots, d^K\}$ over the image series. We worked with two-channel images where the cytoskeleton is marked with Lifeact-GFP and nuclei are marked with NLS-mCherry. The nuclei can be reliably detected and segmented by simply thresholding the NLS-mCherry channel and performing a morphological filling operation. Alternatively, one could apply a fast machine learning detector such as the one in [6].

Using the nuclei as seed points, somata are segmented as follows. A list of pixels neighboring the current soma segmentation is maintained. At each iteration, the neighbor with the smallest weighted distance to the centroid of the seed nucleus detection $D = \lambda||u - d^k|| + |I(u) - \hat{I}(d^k)|$ is added to the soma so long as $D < Y$, where u is a location in the image, $I(u)$ is the pixel intensity at that location, $\hat{I}(d^k)$ is the mean intensity of detection d^k, and Y is a threshold.

2.2. Efficient Tracking of Nucleus Detections

The tracking algorithm searches through the full set of nuclei detections and iteratively associates the most similar pairs of detections, returning lists of valid detections corresponding to each neuron $\mathcal{X}^i$. This is accomplished by constructing a graph $\mathcal{G} = (\mathcal{D}, \mathcal{E})$ where each node $d_t^k \in \mathcal{D}$ corresponds to a detection. For each detection d_t^k in time step t, edges $e \in \mathcal{E}$ are formed between d_t^k and all past and future detections within a time window W. A weight w_e is assigned to each edge $e^{k,l}$ connecting d_t^k and d_t^l. The weight w_e relates to spatial distances, temporal distances, and a shape measure: $w_e = \alpha||d_{t1}^k - d_{t2}^l|| + \beta|t1 - t2| + \gamma f(\nu_{t1}^k, \nu_{t2}^l)$, where ν^k is a shape feature vector containing d_t^k's area, perimeter, mean intensity, and major and minor axis lengths of a fitted ellipse. f evaluates differences between a feature a extracted from d_t^k and d_t^l as $f(a^k, a^l) = |a^k - a^l|/|a^k + a^l|$. The tracking solution corresponds to a set of edges $\mathcal{E}' \subset \mathcal{E}$ with maximal edge weight Q that forms a set of disconnected tracks $\mathcal{T}$ and minimizes the cost function $\sum_{e \in \mathcal{T}} w_e$.

To minimize this cost function, we adopt a greedy selection algorithm, summarized in Fig. 3, that iteratively selects an edge with minimum cost $\hat{w}_e$ and adds it to the set $\mathcal{L}$ removing future and past connections from the detections $e^{k,l}$ connects. The algorithm iterates until the minimum cost $\hat{w}_e$ is greater than a threshold Q. Each track i is then associated with a neuron identity $\mathcal{X}^i$.

2.3. Neuron Segmentation and Neurite Tree Extraction

Given an image I_t and the set of somata present in it $S_t = \{s_t^1 \ldots s_t^m\}$, our goal is to associate to each pixel u a label $J_t(u)$ that indicates to which neuron (soma) it belongs, if any.

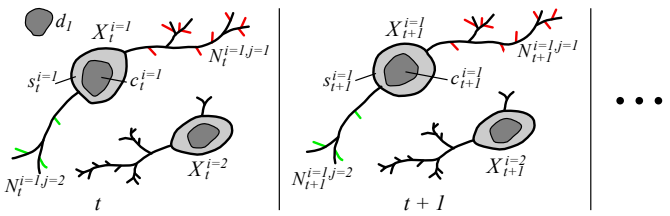

Fig. 2: Neuron tracking notation. At time t a neuron i detection $X_t^i = \{c_t^i, s_t^i, N_t^i\}$ contains a nucleus c_t^i, a soma s_t^i, and a set of neurite-filopodia tuples $N_t^i = \{(n_t^{i,1}, F_t^{i,1}), \ldots, (n_t^{i,j}, F_t^{i,j}), \ldots, (n_t^{i,J}, F_t^{i,J})\}$ which contains J neurites and their associated filopodia shown in red for $j = 1$ and green for $j = 2$. A spurious nucleus detection d_1 is also shown. A neuron i is defined by a time-series of neuron detections $\mathcal{X}^i = \{X_a^i, \ldots, X_t^i, \ldots, X_b^i\}$. The tracking returns a set $\mathcal{X}^i$ for each neuron.

The probability of $J_t(u)$ can be deduced using Bayes' rule,

$$P(J_t(u) = i|S_t, I_t) = \frac{P(S_t, I_t|J_t(u) = i)}{\sum_{\eta=1}^{m} P(S_t, I_t|J_t(u) = \eta)}, \quad (1)$$

where we assume a uniform distribution on $P(J_t(u))$. The numerator is modeled as the probability of the path L that connects maximally pixel u to soma s_t^i, $P(S_t, I_t|J_t(u) = i) = \max_{L:u\to s_t^i} \prod_{\{l_r\}\in L} P(I_t(r)|l_r)$, where l_r are indicator variables for the locations forming the path L. We chose this model since it produces connected components and an optimal maxima can be found by minimizing its negative likelihood using Dijkstra's shortest path.

To optimize this function, we map the image I_t to a graph $\mathcal{G}_t^i = (V, E)$ whose vertices u are the pixels in I_t and whose directed edges $e_{r,v}$ connect each pixel to its four neighbors. We assign to each edge a weight $w_{r,v} = -logP(I_t(v)|v)$. $P(I_t(v)|v)$ represents the probability that a neurite traverses a node v. It is obtained by applying a sigmoid function to the output of the tubularity filter of [7]. The parameters of the sigmoid function are estimated using maximum likelihood. Finally, we define the set of neurite pixels U_n^t as those that connect to any soma with a higher probability than ϵ. We predict their labels as the ones that maximize Eq. 1. The set of pixels associated to neuron X_t^i is the union of the neurites and the soma associated with i, $U_i^t = \{u \in U_n^t | J_t(u) = i\} \cup s_t^i$. To reduce the neurite segmentation to a tree, we skeletonize the neuron and define as root node the pixel of the skeleton closest to the centroid of the nucleus. We instantiate a Minimum Spanning Tree from the root and create a neurite tree whenever the spanning tree exits the soma.

2.4. Neurite Tracking and Filopodia Detection

The identity of neurites is tracked across the frames of the time-lapse videos by applying the algorithm described in Sec 2.2, but using the centroids of the neurite trees instead of the centroids of nuclei, with the additional constraint that edges may only exist between neurites that emanate from the same soma. Filopodia are detected by starting at each leaf node in a neurite and traversing the tree until a branch point is reached. If the distance traversed is less than a threshold T_f, the traversed locations are considered to be filopodia.

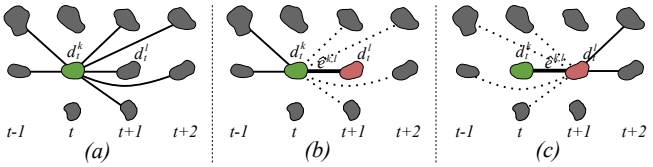

Fig. 3: Efficient tracking by association. *(a)* A graph is built by fully connecting each detection to all future and past detections within a time window W. In this simplified diagram, only d_t^k's edges are shown and W=2. *(b)* Each iteration, the edge $\hat{e}^{k,l}$ with minimum cost $\hat{w}_e$ is added to $\mathcal{E}'$. Edges connecting d_t^k to future detections are removed from $\mathcal{E}$. *(c)* Edges connecting d_t^l to the past are removed from $\mathcal{E}$. The process is repeated until $\hat{w}_e > Q$.

3. EXTRACTING MORPHODYNAMIC FEATURES

Our neuron tracking, segmentation and delineation method produces sets of graphs linking detections, contours, and trees to define each neuron over time. This data structure is not immediately useful for quantifying dynamic behaviors. To facilitate the analysis, we extract a set of *156 informative features* from our data structure to quantify morphodynamics, which are too numerous to list here. A few examples for the nucleus and soma include: area, perimeter, Lifeact-GFP intensity, NLS-mCherry intensity, speed, acceleration, total distance traveled, time spent expanding/contracting, frequency of expansion. For neurites: number of branches, distance from tip to soma, filopodia length, number of filopodia, major axis, minor axis and eccentricity of an ellipse fitted to the neurite, total length, time spent expanding/contracting, frequency of expansion. We also compute change-over-time for each of the features mentioned above (denoted by Δ).

4. RESULTS

We applied our approach to data from a small-scale siRNA screen in which the functions of 5 genes were inhibited: SrGAP2, MAP2K7, RhoA, Trio, and Net. Three siRNAs were applied for each gene, producing a total of 17 experiments including 2 controls. 30 videos per experiment were obtained over the course of 3 days, with images taken at 20× magnification in 10 minute intervals. A total of 510 videos were collected, each containing approximately 100 2-channel images of 696×520 resolution. We tracked and segmented a total of 7,298 neurons (33,213 neurites), extracting morphodynamic features for each. Video were processed in under 210 s, on average, using a notebook computer. The entire screen was processed in just a few hours using conventional PCs.

4.1. Analysis

Our goals were to reproduce the findings of [5], quantify previously observed but unmeasured morphodynamics, and uncover new dynamic behaviors. A brief summary of our findings is provided below and in Fig 4. Reported findings are statistically significant, with p-values $<< 0.05$.

Our analysis confirmed several effects previously observed through static image analysis in [5]. In particular,

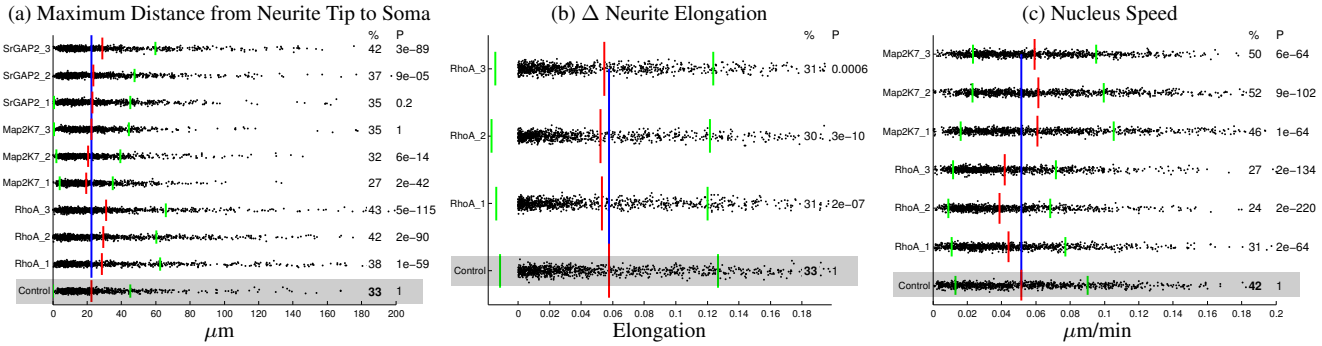

Fig. 4: Morphodynamic analysis of 3 of the 156 informative features extracted through our analysis. The control is marked in gray. Black dots indicate collected data points. Red bars indicate the mean, green bars indicate standard deviation. The control mean is shown by a blue line. Values under the % column show the percentage of data points above the control mean. The P column reports the statisical signifcance measured by the student-t test p-value. *(a)* Our analysis confirmed the finding from [5] that RhoA and SrGAP2 loss results in longer neurites, and Map2K7 loss results in shorter neurites. *(b)* The decrease in mean neurite elongation associated with loss of RhoA quantifies the observation that RhoA loss limits the cell's ability to retract neurites. Neurites of neurons without RhoA produce more lateral branches, therefore their elongation is decreased. *(c)* Our analysis revealed that loss of Map2K7 and RhoA led to an enhancement/retardation of nucleus speed, which was impossible to observe through static analysis.

RhoA loss of function resulted in fewer but longer neurites than the control. SrGap loss was found to have longer neurites, and Map2K7 loss was found to have more neurites but of shorter length. These findings were confirmed by static measures from our experiments: the mean longest neurite length – control 22.6μm, RhoA-3 32μm, SrGap2-1 28.9μm, and Map2K7-1 19.5μm (see Fig. 4a); and by a dynamic measure – the mean number of neurites belonging a neuron over its lifetime: control 3.4, RhoA 3.1, and Map2K7-1 3.9.

It had been previously observed, but never quantified, that loss of SrGap2 function produces a high number of filopodia, and that RhoA loss results in neurites that easily extend but have difficulty retracting. Morphodynamic features from our analysis confirmed these observations. Mean number of filopodia detected per neurite over its lifetime was 6.69 in the control and 8.81 for SrGap-3. The mean change in elongation as measured by an ellipse fitted to the neurite was 5.7% for the control and 5.3% for RhoA-1 (see Fig. 4b). While this difference may seem small, it is statiscially significant due to the large amount of data collected (p-value of 2×10^{-7}).

Our quantitative analysis revealed new morphodynamics which were not obvious to human observers. We found that RhoA function loss slowed neuron motility and Map2K7 increased it. Control cells moved at .30 μm/min, RhoA moved at .23 μm/min, and Map2K7-2 moved at .37 μm/min (see Fig. 4c). We also found that RhoA and SrGap increased the branching of the neurites. Over the course of a neurites lifetime, the maximum number of branches in a control neuron was 14.5, 19.44 for RhoA-3, and 21.39 for SrGap2-3.

5. CONCLUSION

We have described a fully automatic method to track and quantify the morphodynamics of differentiating neurons in fluorescence time-lapse datasets. Our approach is capable of robustly detecting, tracking, and extracting the morphology of the entire neuron including the nucleus, soma, neurites, and filopodia. Previous efforts to analyze high-throughput screens have been limited to static images or simple cell behavior, whereas our approach provides researchers with a rich dynamic analysis of complex cellular behavior in high-throughput time-lapse data. From the rich set of 156 features we extract in our experiments we are able to to 1) corroborate previous findings by biologists, 2) quantify previously observed neuronal behavior and 3) infer new unobserved behaviour, all with strong statistical significance.

Acknowledgments

This work was supported in part by the SNF Sinergia grant "Understanding Brain Morphogenesis", the Madrid-MIT M+Visión consortium for biomedical research, and SystemsX.ch, the Swiss national initiative for Systems Biology, through the SyBIT project.

6. REFERENCES

[1] C. Bakal and et al., "Quantitative Morphological Signatures Define Local Signaling Networks Regulating Cell Morphology," *Science*, vol. 316, pp. 1753–1756, 2007.

[2] C. Collinet and et al., "Systems Survey of Endocytosis by Multiparametric Image Analysis," *Nature*, vol. 464, pp. 243–249, 2010.

[3] M. Held and et al., "Cellcognition: Time-Resolved Phenotype Annotation in High-Throughput Live Cell Imaging," *Nature Methods*, vol. 9, no. 7, pp. 747–754, 2010.

[4] B. Neumann and E. Al, "Phenotypic Profiling of the Human Genome by Time-Lapse Microscopy Reveals Cell Division Genes," *Nature*, vol. 464, pp. 721–727, 2010.

[5] O.C. Pertz, Y. Wang, F. Yang, W. Wang, L.J. Gay, M.A. Gristenko, T.R. Clauss, D.J. Anderson, T. Liu, K.J. Auberry, D.G. Camp, R.D. Smith, and R.L. Klemke, "Spatial Mapping of the Neurite and Soma Proteomes Reveals a Functional Cdc42/rac Regulatory Network," vol. 105, pp. 1931–1936, 2008.

[6] K. Smith, A. Carleton, and V. Lepetit, "Fast Ray Features for Learning Irregular Shapes," in *ICCV*, 2009, pp. 397–404.

[7] A.F. Frangi, W.J. Niessen, K.L. Vincken, and M.A. Viergever, "Multiscale Vessel Enhancement Filtering," *Lecture Notes in Computer Science*, vol. 1496, pp. 130–137, 1998.